Nonreciprocal Magnons and Symmetry-Breaking in the Noncentrosymmetric Antiferromagnet

G. Gitgeatpong,[1,2,3] Y. Zhao,[4,5] P. Piyawongwatthana,[1] Y. Qiu,[5] L. W. Harriger,[5] N. P. Butch,[5] T. J. Sato,[6] and K. Matan[1,2,*]
[1]Department of Physics, Faculty of Science, Mahidol University, Bangkok 10400, Thailand
[2]ThEP, Commission of Higher Education, Bangkok 10400, Thailand
[3]Department of Physics, Faculty of Science and Technology, Phranakhon Rajabhat University, Bangkok 10220, Thailand
[4]Department of Materials Science and Engineering, University of Maryland, College Park, Maryland 20742, USA
[5]NIST Center for Neutron Research, National Institute of Standards and Technology, Gaithersburg, Maryland 20899, USA
[6]IMRAM, Tohoku University, Sendai, Miyagi 980-8577, Japan
(Received 27 February 2017; published 24 July 2017)

Inelastic neutron scattering measurements were performed to study spin dynamics in the noncentrosymmetric antiferromagnet α-$Cu_2V_2O_7$. For the first time, nonreciprocal magnons were experimentally measured in an antiferromagnet. These nonreciprocal magnons are caused by the incompatibility between anisotropic exchange and antisymmetric Dzyaloshinskii-Moriya interactions, which arise from broken symmetry, resulting in a collinear ordered state but helical spin dynamics. The nonreciprocity introduces the difference in the phase velocity of the counterrotating modes, causing the opposite spontaneous magnonic Faraday rotation of the left- and right-propagating spin waves. The breaking of spatial inversion and time reversal symmetry is revealed as a magnetic-field-induced asymmetric energy shift, which provides a test for the detailed balance relation.

DOI: 10.1103/PhysRevLett.119.047201

While symmetry plays a central role in imposing uniformity on the fundamental laws of nature [1,2], symmetry breaking introduces "the texture of the world" [3] by adding layers of complexity to the physical laws. In condensed matter systems, symmetry and a lack of it determine the underlying interactions of the governing Hamiltonian. In particular, the absence of spatial inversion symmetry in magnetic systems causes the relativistic spin-orbit coupling, which gives rise to many intriguing phenomena such as the spin Hall effect [4], topological insulators [5,6], multiferroics [7,8], and noncentrosymmetric superconductors [9,10], to acquire antisymmetric Dzyaloshinskii-Moriya (DM) interactions [11,12].

Spin dynamics can reveal underlying symmetry and symmetry breaking in a system. In an isotropic Heisenberg system, disturbances in the form of magnons, the spin-wave quanta, that embody a wave propagating through a background medium formed by ordered magnetic moments vary in a continuous manner around an ordered spin structure, thus requiring infinitesimal energy as a wave vector approaches a magnetic zone center. However, competing anisotropic interactions arising from broken symmetry can favor a distinct static and dynamic spin state causing a shift of the minimum point of the magnon dispersion to a nonreciprocal wave vector [13]; these magnons are called nonreciprocal magnons. For noncentrosymmetric α-$Cu_2V_2O_7$, the crystal structure breaks spatial inversion symmetry [14,15], and the antiferromagnetic ordering below $T_N = 33.4$ K [16,17] breaks time reversal symmetry. The simultaneous breaking of both symmetries sets the stage for the intertwining electric and magnetic properties [17–21] and for the existence of the nonreciprocal magnons.

In the magnetically ordered state, $S = 1/2$ Cu^{2+} spins in α-$Cu_2V_2O_7$ align antiparallel along the crystallographic a axis forming a collinear structure. In the presence of a magnetic field along the c axis, weak ferromagnetism resulting from the DM-interaction-induced canted moments was observed. When the magnetic field is applied along the a axis, two magnetic transitions appear: one transition at $\mu_0 H_{c1} = 6.5$ T is characterized as the spin-flop transition whereas the other at $\mu_0 H_{c2} = 18.0$ T is a result of the spin flip [22]. Combined density functional theory (DFT) calculations and quantum Monte Carlo simulations suggest a complex spin network shown in Fig. 1(d) [18,22,23]. To the first approximation, the spin Hamiltonian for α-$Cu_2V_2O_7$ can be described by [13]

$$\mathcal{H} = \sum_{i,j} J_{ij}\mathbf{S}_i \cdot \mathbf{S}_j + \sum_{k,l} G_{kl}(S_k^x S_l^x - S_k^y S_l^y - S_k^z S_l^z) + \sum_{k,l} \mathbf{D}_{kl} \cdot (\mathbf{S}_k \times \mathbf{S}_l) - g_e \mu_B \sum_i \mathbf{S}_i \cdot \mathbf{H}, \quad (1)$$

where the summation $\sum_{i,j}$ ($\sum_{k,l}$) is taken over the nearest, second-nearest, and third-nearest neighbors (nearest neighbors). The first term represents the isotropic exchange interactions, where J_1, J_2, and J_3 depicted in Fig. 1(d) are all antiferromagnetic with $J_1 \sim J_2 < J_3$ [22]. The second term represents the anisotropic exchange interaction G_1, which arises from the multiorbital correlation effect caused by the relativistic spin-orbit coupling and multiorbital

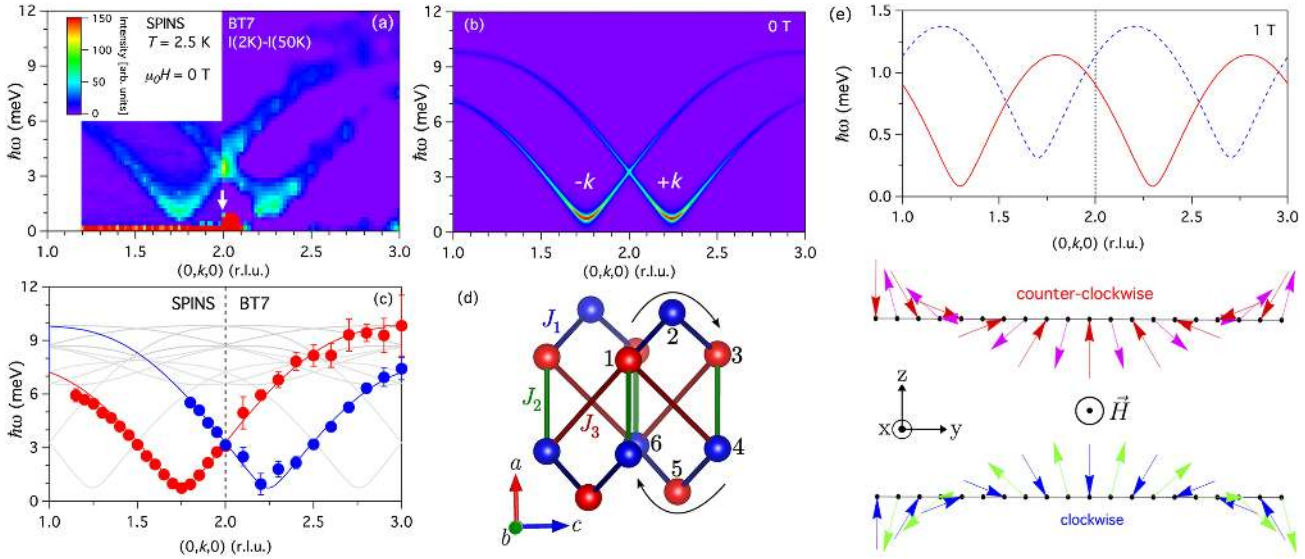

FIG. 1. [(a)–(c)] The zero-field magnetic excitations in α-$Cu_2V_2O_7$. (a) The contour map, which is constructed from a series of constant-$\mathbf{Q}$ scans taken at SPINS for $k < 2$ and at BT7 for $k > 2$, shows two dispersive branches of the excitations centered around (0, 1.75, 0) and (0, 2.25, 0). The BT7 contour map represents the intensity difference between the data measured at 2 and 50 K. An arrow denotes the magnetic Bragg reflection at (0, 2, 0). (b) The contour map of the calculated dynamical structure factor $S(\mathbf{Q}, \hbar\omega)$ representing the spin-wave intensity along $(0, k, 0)$ was calculated using the obtained fit parameters. (c) The spin-wave dispersions of all 16 branches are shown in grey, while red and blue lines represent the most intense branches. The data points were obtained from resolution-convolution fitting of the constant-$\mathbf{Q}$ scans. Error bars denote standard derivations throughout the article. (d) The spin network of α-$Cu_2V_2O_7$ is formed by three dominant exchange interactions J_1, J_2, and J_3. Red and blue spheres represent two spin sublattices, which are parallel and antiparallel to the a axis, respectively. Arrows and spin labels denote the order of the cross product. (e) The magnetic excitations of the spin-chain model in an applied magnetic field along the x axis [Eq. (S1)] were calculated with $S = 1/2$, $J = 1$ meV, $G = 0.26$ meV, $D = 1.0$ meV, and $H = 1$ T (Supplemental Material [25]). Dynamical spin structures, which show the counterclockwise and clockwise rotation of the fluctuating spins around the field direction ($+x$ direction), correspond to the solid red and dashed blue modes, respectively.

hybridization [13,19,24]. The third term denotes the antisymmetric Dzyaloshinskii-Moriya interactions $\mathbf{D}_1$, which result from the absence of the inversion center between the nearest-neighbor spins [11,12]. The last term represents spins in an external magnetic field, where $g_e = -2$ is the electron spin g-factor, μ_B is the Bohr magneton, and $\mathbf{H}$ is the magnetic field applied parallel to the crystallographic a axis.

The anisotropic exchange interaction stabilizes the collinear antiferromagnetic spin structure and introduces an energy gap to the magnon excitations, whereas the a component of the DM vector favors a helical spin structure in the bc plane and determines the incommensurate wave vector of the helical modulation. Because of the competition between these two terms, spin fluctuations of the dynamic state may not be around the static spin structure, resulting in the nonreciprocal magnons. In this Letter, we report the realization of such nonreciprocal magnons in noncentrosymmetric α-$Cu_2V_2O_7$. The DM interaction lifts the degeneracy of clockwise and counterclockwise magnon modes, whereas the applied magnetic field causes an asymmetric energy shift between the two counterrotating modes.

Single crystals of α-$Cu_2V_2O_7$ were grown using the method described in Ref. [16]. Inelastic neutron scattering measurements were conducted to study spin dynamics using the thermal-neutron triple-axis spectrometer BT7 [26], the cold-neutron triple-axis spectrometer SPINS, the Multi Axis Crystal Spectrometer [27], and the Disk Chopper time-of-flight Spectrometer [28], all of which are located at the NIST Center for Neutron Research (NCNR), Gaithersburg, Maryland, USA. The details of the neutron scattering experiments are described in Supplemental Material [25].

An intensity contour map as a function of energy transfer $\hbar\omega$ and momentum transfer $\mathbf{Q}$ measured in a zero magnetic field at the base temperature along $(0, k, 0)$ shows two branches of spin-wave excitations symmetrically centered on both sides of the magnetic zone center (0, 2, 0), where a magnetic Bragg reflection is observed [Fig. 1(a)]. The two magnon modes correspond to the clockwise and counterclockwise rotation of spins bonded by J_1 with G_1 and $\mathbf{D}_1$ along the $[0\bar{1}\,\bar{1}]$ and $[0\bar{1}1]$ uniform zigzag chains (Fig. S9). The degeneracy of these two modes is lifted by the DM interaction, which causes the observed symmetric shift of the magnon modes to the $-k$ (left) and $+k$ (right) side of the zone center [Fig. 1(b)]. The $+k$ ($-k$) mode corresponds to the counterclockwise rotation along the b axis but clockwise (counterclockwise) along the spin-chain directions (see Supplemental Material [25]). Constant-energy contour maps of scattering intensity (Fig. S1) covering a wider

range in the $(0kl)$ and $(hk0)$ scattering planes confirm that the nonreciprocity of the magnon dispersion, which was not observed in the recent inelastic neutrons scattering on a powder sample [23], is only along $(0, k, 0)$, which is consistent with linear spin-wave calculations [Figs. S1(g)–S1(j)], as discussed later. The energy of both modes increases steadily with roughly the same slope up to about 10 meV, and they cross at the zone center at $\hbar\omega \sim 3$ meV. The absence of crossing avoidance suggests that the counterrotating excitations are decoupled. The energy scan measured at the high-resolution cold-neutron spectrometer SPINS yields the gap energy $\Delta = 0.75(6)$ meV at (0, 1.75, 0) [Fig. S2(d)]. The gap energy as a function of temperature correlates with the decrease of the order parameter and the peak width becomes broader, which is indicative of shorter lifetime, as temperature increases toward T_N (Fig. S3). These results confirm that the excitations are due to the fluctuations of the ordered magnetic moments. The nonreciprocal magnons were recently observed in the field-induced ferromagnetic phase of noncentrosymmetric MnSi, where the shift of the single, nondegenerate magnon mode is asymmetric depending on the field direction [29], in contrast to the symmetric shift in the antiferromagnet at zero field observed in this study.

To quantitatively describe the observed magnon dispersion in α-$Cu_2V_2O_7$, we employed linear spin-wave calculations [30], which are described in Supplemental Material [25]. The calculated magnons consist of 16 modes, denoted by the grey lines in Figs. 1(c), S4(a), and S4(b). However, only two modes, which were experimentally observed in Fig. 1(a) and theoretically confirmed in Figs. 1(b), S4(c), and S4(d), were selected to fit the measured dispersion. The data points in Fig. 1(c) show the measured magnon dispersion along $(0, k, 0)$ obtained from the constant-$\mathbf{Q}$ scans (Fig. S2). The dispersion along $(h, 1.75, 0)$ and $(0, 2, l)$ (Fig. S4) as well as the field dependence of the energy gap [Fig. 4(d)] were also measured and used in the global fit to obtain the relevant Hamiltonian parameters in Eq. (1). The ratio $J_1 : J_2 : J_3$ was fixed to the result obtained from the DFT calculations of 1.00 : 1.12 : 2.03 [22]. The minimal model, which includes three isotropic exchange interactions, the anisotropic exchange interaction G_1, and the uniform DM vector $\mathbf{D}_1 = (D_{1a}, 0, 0)$, is able to capture the magnon nonreciprocity along $(0, k, 0)$ and the dispersion as shown by the solid lines in Figs. 1(c), S4(a), and S4(b). The obtained fitted parameters are $J_1 = 2.67(1)$ meV, $J_2 = 2.99$ meV, $J_3 = 5.42$ meV, $G_1 = 0.282(1)$ meV, and $D_{1a} = 2.79(1)$ meV. The value of the DM parameter with $D_{1a}/J_1 \sim 1$ is much higher than that measured in other $S = 1/2$ Cu^{2+} spin systems [31,32], suggesting the exceptionally strong spin-orbit coupling.

The symmetry between the counterclockwise and clockwise modes is broken in the presence of the applied magnetic field as the electron spins precess under the perpendicular field, and if the spin rotation is in the same

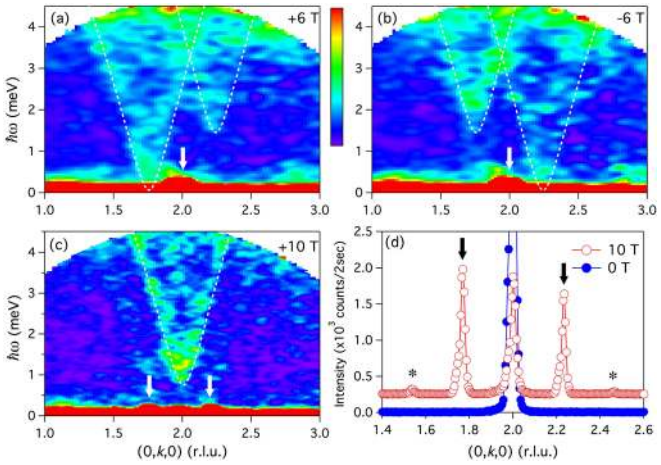

FIG. 2. Spin-wave excitations in a magnetic field at 1.5 K. (a)–(c) show the energy-momentum contour maps measured at 6, −6, and 10 T, respectively. Dashed lines denote the most intense branches resulting from the spin-wave calculations. (d) shows the magnetic Bragg peak measured along $(0, k, 0)$ below and above the spin-flop transition (similar data measured at different fields are reported in Ref. [22]). Arrows denote the magnetic Bragg peaks, and asterisks (*) indicate the second harmonic reflections.

(opposite) sense as (to) the spin precession, or counterclockwise (clockwise) rotation, the excitation energy becomes lower (higher) as illustrated for the spin-chain model in Fig. 1(e) (also see Supplemental Material [25]). Experimentally, for α-$Cu_2V_2O_7$ when the applied field is positive along the a axis ($\mu_0 H = +6$ T), the $+k$ mode (clockwise rotation along the zigzag chain) is shifted upward whereas the $-k$ mode (counterclockwise rotation) is shifted downward [Fig. 2(a)]; on the other hand, if the field is negative ($\mu_0 H = -6$ T), the shift of the dispersion reverses [Fig. 2(b)]. Spin-wave calculations confirm the energy shift in the presence of the field as shown in Fig. S5. The energy scans at +1 T (+2 T) shown in Fig. 3(a) [3(b)] display the asymmetric shift of the gap energy at (0, 1.75, 0) and (0, 2.25, 0). Figure 3(c) depicts the same energy shift of the $+k$ and $-k$ modes when the field of the same magnitude is oppositely aligned. The gap energy as a function of field [Fig. 3(d)] shows a linear relation, consistent with the spin-chain model (Supplemental Material [25]), with a negative slope for (0, 1.75, 0) and positive slope for (0, 2.25, 0). Extrapolating the linear relation to intersect the horizontal axis yields the critical field $\mu_0 H_{c1}$ of $\pm 6.61(2)$ T, at which the energy gaps at $(0, 2 \mp 0.25, 0)$ close and the spin-flop transition occurs [22].

When the applied field is increased from +6 to +10 T, the magnetic Bragg reflection at (0, 2, 0), indicated by the arrow in Fig. 2(a), moves to the incommensurate wave vectors $(0, 2 \pm \delta, 0)$ where $\delta \sim 0.23$, as denoted by the pair of arrows in Figs. 2(c) and 2(d). The transfer of the Bragg intensity documented in Fig. 2(d) occurs at the spin-flop transition reported at $\mu_0 H_{c1} = 6.5$ T [22], and is consistent with the transition from the collinear spin structure to the

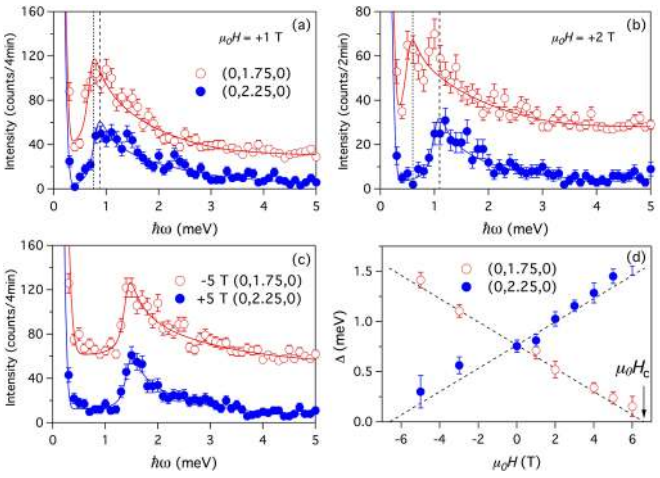

FIG. 3. Constant-**Q** scans were measured at (0, 1.75, 0) and (0, 2.25, 0) at (a) 1 and (b) 2 T. The dashed and dotted lines denote positions of the energy gap. In (c), the scan at (0, 1.75, 0) and −5 T is compared with that at (0, 2.25, 0) and +5 T, which shows the same shift in energy. All (0, 1.75, 0) data are shifted for clarity. The gap energy as a function of field at (0, 1.75, 0) and (0, 2.25, 0) is shown in (d). The critical field is labeled by μ_0H_c, at which the energy gap vanishes.

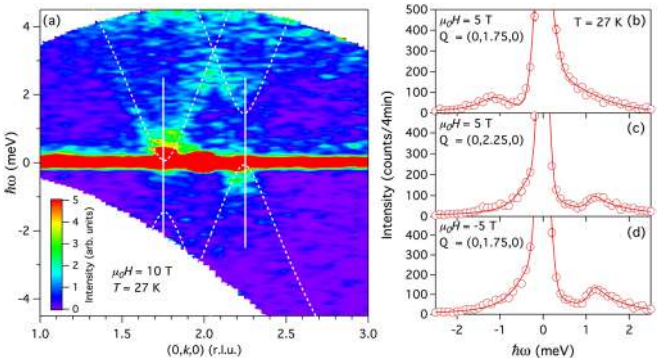

FIG. 4. Detailed balance relation of the scattering intensity. (a) The energy-momentum contour map of the scattering intensity was measured at $T = 27$ K with (a) $\mu_0H = +10$ T and [(b) and (c)] $\mu_0H = \pm 5$ T, which put the system in the collinear antiferromagnetic state in the phase diagram (Fig. S10). The solid lines denote the constant-**Q** scans, which were performed to investigate the negative-energy-transfer and positive-energy-transfer excitations for (b) $\mathbf{Q} = (0, 1.75, 0)$ and $\mu_0H = +5$ T, (c) $\mathbf{Q} = (0, 2.25, 0)$ and $\mu_0H = +5$ T, and (d) $\mathbf{Q} = (0, 1.75, 0)$ and $\mu_0H = -5$ T.

helical spin structure with the majority of the spin component being in the bc plane. The harmonic reflections at roughly $(0, 2 \pm 2\delta, 0)$ indicated by the asterisks in Fig. 2(d) substantiate the incommensurate modulation of the helical structure. The spin-wave excitations in the spin-flop state show the minimum at (0, 2, 0) [Fig. 2(c)] indicative of the reciprocal magnons. Hence, while the collinear spin structure below μ_0H_{c1} hosts the nonreciprocal magnons, the helical spin structure above μ_0H_{c1} gives rise to the reciprocal magnons with the polarization most likely along the a axis, highlighting the competitive nature of the anisotropic exchange and antisymmetric DM interactions.

The asymmetry between the $-k$ and $+k$ modes provides a great opportunity to verify the well-known detailed balance relation for the dynamical structure factor, which can be described by [33]

$$S(-\mathbf{q}, -\hbar\omega) = e^{-\hbar\omega/k_BT} S(\mathbf{q}, \hbar\omega), \tag{2}$$

where k_B is the Boltzmann constant, and the momentum transfer **q** is measured from the zone center. The breaking of inversion symmetry in the α-$Cu_2V_2O_7$ crystal structure and of time reversal symmetry due to the applied field introduces the asymmetry between the clockwise and counterclockwise magnon modes, with the result that $S(-\mathbf{q}, \pm\hbar\omega) \neq S(+\mathbf{q}, \pm\hbar\omega)$. The energy-momentum contour map was measured at 27 K and 10 T, where the system is in the collinear antiferromagnetic states as the critical field μ_0H_{c1} increases to ∼15 T at $T \sim 25$ K (Fig. S10). The elevated temperature is necessary to populate magnons and facilitate the neutron-energy-gain (negative-energy-transfer) scattering process. Figure 4(a) illustrates the asymmetry upon the sign reversal of **q** and $\hbar\omega$ separately, reflecting broken inversion and time reversal symmetry, respectively. The detailed measurements of the constant-**Q** scans extended to negative energy shown in Figs. 4(b)–4(d) display the asymmetry between the neutron-energy-gain and neutron-energy-loss scattering intensity satisfying the detailed balance relation in Eq. (2); the asymmetry is reversed when the momentum transfer changes from $+\mathbf{q}$ to $-\mathbf{q}$ and vice versa [Figs. 4(b) and 4(c)], and when the field direction is flipped [Figs. 4(b) and 4(d)].

The magnon nonreciprocity due to the DM interaction causes the clockwise and counterclockwise modes to acquire different phase velocities resulting in the rotation of the magnon polarization, called the spontaneous magnonic Faraday effect. In contrast to a ferromagnet [34–36], the magnonic Faraday rotation in the antiferromagnet is opposite for the left- and right-propagating spin waves, thus giving rise to the net nonreciprocal phase flow in thermal equilibrium. Taking the role of the DM interaction, an external electric field, which breaks inversion symmetry and lifts the degeneracy of the two counterrotating modes, can cause magnon nonreciprocity and lead to the electric-field-induced magnonic Faraday effect, which may find applications in the spin-wave field-effect transistor [37].

α-$Cu_2V_2O_7$ emerges as the prototypical noncentrosymmetric antiferromagnet, in which the nonreciprocal magnons were observed. Our work provides the fundamental understanding of the interconnection between the broken underlying symmetries (spatial inversion and time reversal), which give rise to the anisotropic terms in the spin Hamiltonian, and the asymmetry of the magnon dispersion. The controllability of the magnon reciprocity and energy shift using the electric and magnetic fields, respectively,

could potentially lead to applications in future magnonic devices.

We thank Y. Motome for fruitful discussion. Work at Mahidol University was supported in part by the Thailand Research Fund Grant No. RSA5880037 and the Thailand Center of Excellence in Physics (ThEP). Access to MACS was provided by the Center for High Resolution Neutron Scattering, a partnership between the National Institute of Standards and Technology and the National Science Foundation under Agreement No. DMR-1508249. Work at IMRAM was partly supported by a Grant-In-Aid for Scientific Research (Grant No. 24224009) from the Japan Society for the Promotion of Science (JSPS), and by the research program "Dynamic alliance for open innovation bridging human, environment, and materials."

*kittiwit.mat@mahidol.ac.th

[1] R. P. Feynman, R. B. Leighton, and M. L. Sands, *The Feynman Lectures on Physics* (Addison-Wesley Publishing Co., Inc., Reading, Massachusetts, 1963), Vol. 1, Chap. 52.
[2] E. Noether, Gott. Nachr. **1918**, 235 (1918); E. Noether, Transp. Theory Stat. Phys. **1**, 186 (1971).
[3] D. J. Gross, Proc. Natl. Acad. Sci. U.S.A. **93**, 14256 (1996).
[4] J. Sinova, S. O. Valenzuela, J. Wunderlich, C. H. Back, and T. Jungwirth, Rev. Mod. Phys. **87**, 1213 (2015).
[5] X.-L. Qi and S.-C. Zhang, Rev. Mod. Phys. **83**, 1057 (2011).
[6] M. Z. Hasan and C. L. Kane, Rev. Mod. Phys. **82**, 3045 (2010).
[7] S. Dong, J.-M. Liu, S.-W. Cheong, and Z. Ren, Adv. Phys. **64**, 519 (2015).
[8] M. Fiebig, T. Lottermoser, D. Meier, and M. Trassin, Nat. Rev. Mater. **1**, 16046 (2016).
[9] E. Bauer, G. Hilscher, H. Michor, C. Paul, E. W. Scheidt, A. Gribanov, Y. Seropegin, H. Noel, M. Sigrist, and P. Rogl, Phys. Rev. Lett. **92**, 027003 (2004).
[10] *Noncentrosymmetric Superconductors*, Lecture Notes in Physics Vol. 847, edited by E. Bauer and M. Sigrist (Springer Berlin Heidelberg, Berlin, Heidelberg, 2012).
[11] I. Dzyaloshinsky, J. Phys. Chem. Solids **4**, 241 (1958).
[12] T. Moriya, Phys. Rev. **120**, 91 (1960).
[13] S. Hayami, H. Kusunose, and Y. Motome, J. Phys. Soc. Jpn. **85**, 053705 (2016).
[14] C. Calvo and R. Faggiani, Acta Crystallogr. Sect. B **31**, 603 (1975).
[15] P. Robinson, J. Hughes, and M. Malinconico, Am. Mineral. **72**, 397 (1987).
[16] G. Gitgeatpong, Y. Zhao, M. Avdeev, R. O. Piltz, T. J. Sato, and K. Matan, Phys. Rev. B **92**, 024423 (2015).
[17] Y. W. Lee, T. H. Jang, S. E. Dissanayake, S. Lee, and Y. H. Jeong, Europhys. Lett. **113**, 27007 (2016).
[18] J. Sannigrahi, S. Bhowal, S. Giri, S. Majumdar, and I. Dasgupta, Phys. Rev. B **91**, 220407 (2015).
[19] S. Hayami, H. Kusunose, and Y. Motome, Phys. Rev. B **90**, 024432 (2014).
[20] S. Hayami, H. Kusunose, and Y. Motome, J. Phys. Soc. Jpn. **84**, 064717 (2015).
[21] C. Ederer and N. A. Spaldin, Phys. Rev. B **76**, 214404 (2007).
[22] G. Gitgeatpong, M. Suewattana, A. Miyake, M. Tokunaga, P. Chanlert, N. Kurita, H. Tanaka, T. J. Sato, Y. Zhao, and K. Matan, Phys. Rev. B **95**, 245119 (2017).
[23] A. Banerjee, J. Sannigrahi, S. Bhowal, I. Dasgupta, S. Majumdar, H. C. Walker, A. Bhattacharyya, and D. T. Adroja, Phys. Rev. B **94**, 144426 (2016).
[24] S. Hayami, H. Kusunose, and Y. Motome, J. Phys. Condens. Matter **28**, 395601 (2016).
[25] See Supplemental Material at http://link.aps.org/supplemental/10.1103/PhysRevLett.119.047201 for the details and results of neutron scattering experiments, spin-wave calculations, and nonreciprocal magnons in an antiferromagnetic spin chain.
[26] J. W. Lynn, Y. Chen, S. Chang, Y. Zhao, S. Chi, W. Ratcliff, B. G. Ueland, and R. W. Erwin, J. Res. Natl. Inst. Stand. Technol. **117**, 61 (2012).
[27] J. A. Rodriguez, D. M. Adler, P. C. Brand, C. Broholm, J. C. Cook, C. Brocker, R. Hammond, Z. Huang, P. Hundertmark, J. W. Lynn, N. C. Maliszewskyj, J. Moyer, J. Orndorff, D. Pierce, T. D. Pike, G. Scharfstein, S. A. Smee, and R. Vilaseca, Meas. Sci. Technol. **19**, 034023 (2008).
[28] J. Copley and J. Cook, Chem. Phys. **292**, 477 (2003).
[29] T. J. Sato, D. Okuyama, T. Hong, A. Kikkawa, Y. Taguchi, T.-h. Arima, and Y. Tokura, Phys. Rev. B **94**, 144420 (2016).
[30] K. Yosida, *Theory of Magnetism* (Springer Science & Business Media, New York, 1996).
[31] T. Thio and A. Aharony, Phys. Rev. Lett. **73**, 894 (1994).
[32] J. Z. Zhao, X. Q. Wang, T. Xiang, Z. B. Su, and L. Yu, Phys. Rev. Lett. **90**, 207204 (2003).
[33] G. L. Squires, *Introduction to the Theory of Thermal Neutron Scattering* (Cambridge University Press, Cambridge, 1978).
[34] H. T. Nembach, J. M. Shaw, M. Weiler, E. Jué, and T. J. Silva, Nat. Phys. **11**, 825 (2015).
[35] K. Di, V. L. Zhang, H. S. Lim, S. C. Ng, M. H. Kuok, J. Yu, J. Yoon, X. Qiu, and H. Yang, Phys. Rev. Lett. **114**, 047201 (2015).
[36] J. H. Kwon, J. Yoon, P. Deorani, J. M. Lee, J. Sinha, K. J. Lee, M. Hayashi, and H. Yang, Sci. Adv. **2**, e1501892 (2016).
[37] R. Cheng, M. W. Daniels, J.-G. Zhu, and D. Xiao, Sci. Rep. **6**, 24223 (2016).